HEP/123-qed

Numerical simulation of deformable drops with soluble surfactant: Pair interactions and coalescence in shear flow

H. Zhou, V. Cristini,* and C. W. Macosko

Department of Chemical Engineering and Materials Science,

University of Minnesota,

421 Washington Ave. S.E.,

Minneapolis, MN 55455

J. Lowengrub

School of Mathematics,

University of Minnesota

(Dated: November 14, 2002)

Abstract

We study numerically the dynamics of deformable drops in the presence of surfactant species both on the drop-matrix interfaces and in the bulk fluids using a novel 3D adaptive finite-element method. The method is based on unstructured adaptive triangulated and tetrahedral meshes that discretize the interfaces and the bulk respectively, and on an efficient parallelization of the numerical solvers. We use this method to investigate the effects of surfactants on drop-drop interactions in shear flow. The simulations account for surfactant effects through a nonlinear Langmuir equation of state and through adsorption/desorption laws describing the transport between bulk and interface. Van der Waals forces responsible for coalescence are included. For clean drops (no surfactant), our simulations confirm (for the first time to our knowledge) a well known theoretical result [1] for the dependence of the critical capillary number–below which coalescence occurs–on the drop radius with an exponent $-4/9$.

Our results reveal a non-monotonic dependence of the critical capillary number Ca_c on the surface coverage of surfactant. Marangoni stresses prevent drop approach thus decreasing Ca_c with respect to the clean-drop case. However, at large coverages close to the maximum packing of surfactant molecules, surfactant redistribution is prohibited (the surfactant is nearly incompressible) and thus the effect of Marangoni stresses is weakened, leading to an increase of Ca_c. In some cases, Ca_c at high coverages is even larger than in the clean-drop case: surfactant near-incompressibility hinders drop deformation and thus coalescence can occur at higher capillary number.

Finally, our results also reveal a non-monotonic dependence of Ca_c on surfactant solubility in the bulk. At moderate surfactant concentration, diffusion in the bulk decreases surfactant redistribution on the interface and thus weakens Marangoni stresses resulting in higher Ca_c than in the insoluble case. However, when the surfactant bulk concentration is large, high adsorption fluxes maintain a higher surface concentration in equilibrium than for the insoluble case, thus resulting in larger drop deformation and in lower Ca_c.

PACS numbers: 47.15.Gf, 47.55.Dz

*Corresponding author. Present address: Department of Biomedical Engineering, University of California at Irvine, Irvine, CA 92697-2715. Email: cristini@math.uci.edu.

I. INTRODUCTION

The microstructure of emulsions and polymer blends depends strongly on the coalescence events that occur during processing. Surfactants and compatibilizers (block co-polymers) are used to prevent coalescence events and stabilize the size distributions. The effect of surfactants on drop-drop collisions and coalescence has been investigated theoretically (e.g., see [2–6]) and experimentally (e.g., [7, 8]). To our knowledge, no numerical investigation has been performed.

Under the assumption that steric effects associated to the finite size of the surfactant molecules and dissipation associated to surface viscosity can be neglected, three main mechanisms are responsible for the observed inhibition of coalescence:

1. the *average* reduction in surface tension associated to the presence of surfactants, resulting in enhanced drop deformation and thus stronger repulsive hydrodynamic forces that prevent drop-drop approach;

2. the nonuniform capillary pressure (normal stresses) on the drop surface due to *redistribution* of surfactant, also resulting in enhanced deformation;

3. the Marangoni stresses (tangential forces) associated to redistribution of surfactant, and resulting in repulsive forces on the drops [2, 3, 5].

Recent experiments by Leal and coworkers [7] and by Lyu *et al.* [8] confirmed that coalescence is strongly prevented. However, Leal and coworkers [7] found a non-monotonic dependence of the critical capillary number Ca_c (below which coalescence occurs) on the surfactant coverage in flows with a combination of shear and extension. At small coverage, surfactants strongly reduce Ca_c with respect to the clean drops (no surfactant) case. However, at large coverage Ca_c increases again towards the clean-drop value.

In this paper, we investigate drop collisions using adaptive finite-element simulations. Our adaptive numerical method allows us to accurately and efficiently describe the drop deformation and the drop-drop near-contact interactions. We focus on shear flow which is very important in blend processing but difficult to study experimentally. Our accurate simulations allow us to identify the mechanisms leading to the observed nontrivial behavior. In addition, we also study the effect of surfactant solubility in the bulk phases on Ca_c. This effect has not been investigated previously.

II. PROBLEM STATEMENT

A. Governing equations

We consider a pair of equal-sized drops of radius a and viscosity μ_d placed in an infinite matrix fluid of viscosity μ_m. The drops have centers of mass in the xy plane, are symmetric with respect to the origin, and are separated by offsets Δx and Δy. A steady simple shear flow of velocity field $u_\infty = \dot{\gamma} y$ in the x-direction is started at time $t = 0$, where $\dot{\gamma}$ is the shear rate. The drops are initially spherical, and they are pushed toward each other by the compressional component of the flow. A surfactant species is present in the bulk phases with molar concentration C per unit volume and on the interfaces Σ with concentration Γ per unit area. Under the assumption of zero Reynolds number, which typically applies to high viscosity fluids (e.g., polymers), the governing equations for flow in both the drops and the matrix are the Stokes equations:

$$\nabla \cdot \mathbf{T} + \mathbf{f} = \mathbf{0}, \qquad \nabla \cdot \mathbf{u} = 0, \tag{1}$$

where

$$\mathbf{T} = -p\mathbf{I} + \mu_i \left(\nabla \mathbf{u} + \nabla \mathbf{u}^T \right), \qquad i = d, m, \tag{2}$$

is the stress tensor, p and $\mathbf{u}$ are the pressure and velocity fields, $\mathbf{I}$ is the identity tensor,

$$\mathbf{f}(\mathbf{x}) = -\frac{6A}{\pi^2} \int_{\Omega_d} \frac{\mathbf{x} - \mathbf{x}'}{|\mathbf{x} - \mathbf{x}'|^8} \mathrm{d}\mathbf{x}' \tag{3}$$

is the local van der Waals attractive force per unit volume at position $\mathbf{x}$ inside each drop [9], where the integration is performed over the volume of the other drop (Ω_d), and A is the Hamaker constant. Note that $\mathbf{f} = 0$ in the matrix fluid.

The boundary conditions are

$$[\mathbf{u}] = 0, \qquad [\mathbf{T} \cdot \mathbf{n}] = \sigma \kappa \mathbf{n} - \nabla_s \sigma, \qquad \text{on } \Sigma, \tag{4}$$

and

$$\mathbf{u} \to \mathbf{u}_\infty, \quad \text{as } |\mathbf{x}| \to \infty, \tag{5}$$

where the square brackets indicate the jump of a quantity, at the interface Σ, from the drop to the matrix phase, σ is the local surface tension on the interface, κ is the local total curvature of Σ such that $\kappa = 2$ on a sphere of radius 1, $\mathbf{n}$ is the outward normal of the

interface, $\nabla_s = (\mathbf{I} - \mathbf{nn}) \cdot \nabla$ is the surface gradient. In the stress boundary condition, the first term on the right-hand side is the capillary pressure (normal stress), and the second term is the Marangoni stress (tangential to the interface). The local surface tension σ at any position on the interface is related to the surface concentration Γ of surfactant by the nonlinear Langmuir's equation of state [10]:

$$\sigma = \sigma_0 + RT\Gamma_\infty \ln\left(1 - \Gamma/\Gamma_\infty\right), \tag{6}$$

where σ_0 is the surface tension for a clean ($\Gamma = 0$) interface, Γ_∞ is the maximum surfactant coverage, R is the ideal gas constant and T is the Kelvin temperature.

The distribution of the surface concentration of surfactant is governed by the surface convection-diffusion equation [11, 12]:

$$\frac{\partial \Gamma}{\partial t} + \nabla_s \cdot (\mathbf{u}_s \Gamma) + \kappa \Gamma u_n = D_s \nabla_s^2 \Gamma + q_{chem} + q_f, \tag{7}$$

where t is time, $\mathbf{u}_s = (\mathbf{I} - \mathbf{nn}) \cdot \mathbf{u}$ and $u_n = \mathbf{n} \cdot \mathbf{u}$ are the tangential and normal velocities respectively, D_s is the surface diffusion constant for surfactant, q_{chem} is the source term that accounts for the formation of surfactant at the interface by chemical reaction (e.g., reactive compatibilization), and q_f is the flux of surfactant from the bulk phases to the interfaces by adsorption-desorption:

$$q_f = \sum_{i=d,m} k_{a,i} \left(C_{s,i} \left(\Gamma_\infty - \Gamma\right) - \beta_i \Gamma\right). \tag{8}$$

Here a unimolecular adsorption-desorption process is assumed and Langmuir's kinetic laws are used [13]: $k_{a,i}$ and $k_{a,i}\beta_i$ are adsorption and desorption kinetic parameters and $C_{s,i}$ are the limit value at the interface of the bulk concentration of surfactant C.

The bulk concentration of surfactant obeys the bulk convection-diffusion equation [13]:

$$\frac{\partial C}{\partial t} + \mathbf{u} \cdot \nabla C = D_i \nabla^2 C, \qquad i = d, m, \tag{9}$$

where the D_i are the diffusion constants in the two phases. The boundary conditions at the interfaces couple the bulk transport equation (9) and the surface transport equation (7):

$$[D \nabla C \cdot \mathbf{n}] = q_f, \quad \text{on } \Sigma, \tag{10}$$

where $D = D_d$ in the drops and D_m in the matrix. In the far field, we have

$$C \to C_\infty, \quad \text{as } |\mathbf{x}| \to \infty, \tag{11}$$

where C_∞ is the uniform bulk concentration of surfactant away from the drops. The initial condition for the bulk concentration is:

$$C = C_\infty, \quad \text{at } t = 0. \tag{12}$$

In the special case of very viscous fluids and large surfactant molecules (e.g., for polymeric fluids with block co-polymers on the interfaces), the surfactant can be assumed to be insoluble in the bulk phases ($C = 0$), non-diffusing ($D_s = 0$), and simply convected on the interfaces by the flow ($q_f = 0$, and $q_{chem} = 0$ in the absence of chemical reaction). When surfactant molecules are soluble in the bulk fluids, our formulation applies for concentrations $C_\infty < C_{\rm CMC}$, where $C_{\rm CMC}$ is the concentration at which micelles form. Also, any steric effects associated to the finite size of the molecules are neglected.

B. Dimensionless formulation

We make the problem dimensionless by using the following characteristic quantities: the drop radius a for length, the inverse shear rate $\dot\gamma^{-1}$ for time, C_∞ for the bulk concentration of surfactant, the surface concentration Γ_e in equilibrium with C_∞ for Γ, and the corresponding equilibrium surface tension $\sigma_e = \sigma(\Gamma_e)$ for σ. The equilibrium surface concentration is obtained by setting $q_f = 0$ in equation (8). In the following, we neglect surfactant solubility in the drop phases, and chemical reaction at the interface. The equilibrium surfactant concentration is

$$\Gamma_e = \frac{\Gamma_\infty}{1 + \beta/C_\infty}; \tag{13}$$

herein the subscript m is dropped for simplicity.

The relevant dimensionless parameters for drop deformation are the capillary number

$$Ca = \frac{\mu_m \dot\gamma a}{\sigma_e}, \tag{14}$$

which represents the strength of the flow relative to the capillary forces, and the viscosity ratio $\lambda = \mu_d/\mu_m$, which we will set to 1 in the work presented here. To measure the magnitude of van der Waals forces responsible for drop coalescence, relative to capillary forces, we introduce a new dimensionless parameter, the Hamaker number, as follows:

$$Ha = \frac{6A}{\pi^2 \sigma_e a^2}. \tag{15}$$

The dimensionless parameters that characterize the surfactant at equilibrium are the surfactant elasticity, which we define here as

$$E_0 = \frac{RT\Gamma_\infty}{\sigma_0}, \tag{16}$$

and the dimensionless surface coverage

$$c = \frac{\Gamma_e}{\Gamma_\infty}. \tag{17}$$

Note that $c < 1$ and that for a clean drop $c = 0$ and in this case $\sigma_e = \sigma_0$ in the definitions (14) and (15) of the capillary number and Hamaker number. We use definition (16) for the surfactant elasticity based on the clean surface tension σ_0 in contrast to the usual definition that uses σ_e [14]. This allows us to vary the parameters E_0 and c independently. Here, we will use the typical value of elasticity $E_0 \approx 0.2$.

The dimensionless parameters associated to the convection-diffusion equations are [13] the Peclet numbers

$$Pe = \frac{\dot{\gamma}a^2}{D}, \quad Pe_s = \frac{\dot{\gamma}a^2}{D_s} \tag{18}$$

for matrix and interface respectively, the Hatta number

$$\alpha = k_a C_\infty/\dot{\gamma}, \tag{19}$$

characterizing the ratio between the adsorption/desorption flux and the advective flux, the Langmuir number

$$La = \frac{C_\infty}{\beta}, \tag{20}$$

and the dimensionless adsorption length

$$K = \frac{\Gamma_\infty}{aC_\infty}. \tag{21}$$

Here we consider that initially the system is in equilibrium, so that $q_f = 0$ and, from equation (13),

$$La = \frac{c}{1-c}. \tag{22}$$

Thus La is not an independent parameter.

The following is a complete list of dimensionless equations for the flow.

$$\nabla \cdot \mathbf{T} + \mathbf{f} = \mathbf{0}, \qquad \nabla \cdot \mathbf{u} = 0, \tag{23}$$

$$\mathbf{T} = -p\mathbf{I} + \lambda_i \cdot (\nabla\mathbf{u} + \nabla\mathbf{u}^T) \tag{24}$$

$$\mathbf{f} = -\frac{Ha}{Ca}\int_\Omega \frac{\mathbf{x}-\mathbf{x}'}{|\mathbf{x}-\mathbf{x}'|^8}\mathrm{d}\mathbf{x}'. \tag{25}$$

$$[\mathbf{u}] = 0, \qquad [\mathbf{T}\cdot\mathbf{n}] = \frac{1}{Ca}(\sigma\kappa\mathbf{n} - \nabla_s\sigma), \qquad \text{on } \Sigma, \tag{26}$$

$$\sigma = \frac{1 + E_0\ln(1-c\Gamma)}{1 + E_0\ln(1-c)} \tag{27}$$

The viscosity ratios $\lambda_i = \lambda$ in the drop fluid and 1 in the matrix fluid. The surfactant equations are

$$\frac{\partial\Gamma}{\partial t} + \nabla_s\cdot(\mathbf{u}_s\Gamma) + \kappa\Gamma u_n = Pe_s^{-1}\nabla_s^2\Gamma + \frac{1}{cK}q_f, \tag{28}$$

$$\frac{\partial C}{\partial t} + \mathbf{u}\cdot\nabla C = Pe^{-1}\nabla^2 C, \tag{29}$$

$$q_f = \left[Pe^{-1}\mathbf{n}\cdot\nabla C\right] = \alpha K(C_s(1-\Gamma c) - \frac{1}{La}\Gamma c). \tag{30}$$

In all the above equations, we use the same notation for the dimensionless variables as for the dimensional variables defined in §II A for simplicity. In the following, we neglect diffusion on the interfaces ($Pe_s = 0$) to investigate the effect of bulk diffusion (in the matrix fluid) alone. Diffusion in the drop fluid is also neglected.

C. Scalings for near-contact drop approach

The theory of film drainage for finite Ca (so that the drop surface in the near contact region is deformed) and clean drops was reviewed by Chesters [1]. It is shown there that, in the absence of van der Waals attractive forces, during drop-drop interaction the drops would reach a minimum distance (gap) as a consequence of a balance of the compressional force imposed by the flow and the repulsive lubrication force, and then separate without coalescing. This minimum gap is $h/a \sim \lambda\mu^{\frac{3}{2}}\dot\gamma^{\frac{3}{2}}a^{\frac{5}{2}}/\sigma_0^{\frac{3}{2}}$, i.e.,

$$\frac{h}{a} \sim \lambda Ca^{\frac{3}{2}}. \tag{31}$$

The separation at which van der Waals forces become important is [1] $h/a \sim (A/(\sigma_0 a^2))^{\frac{1}{3}}$, i.e., using our notation,

$$\frac{h}{a} \sim Ha^{\frac{1}{3}}. \tag{32}$$

By equating (31) and (32) we find that the critical capillary number below which van der Waals forces lead to coalescence scales as

$$Ca_c \sim \lambda^{-\frac{2}{3}} Ha^{\frac{2}{9}}. \tag{33}$$

Formula (33) describes the dependence of critical capillary number for coalescence on the magnitude of van der Waals forces. Note that this scaling was formulated in formula (65) of Ref. [1] in terms of drop radius, thus giving $Ca_c \sim a^{-4/9}$. This scaling is confirmed in our paper using numerical simulations.

D. A typical system

For polymeric fluids, typically the viscosity $\mu \approx 10^3$ Pa s, and the surface tension $\sigma_e \approx 10^{-3}$ N m^{-1}. Thus for shear rates $\dot{\gamma} = 1$ s^{-1} and sub-micron-size drops (e.g., $a = 10^{-7}$ m) we obtain $Ca \approx 0.1$, and, for Hamaker constant $A \approx 10^{-20}$ J, $Ha \approx 10^{-3}$. Thus, drop deformation is modest and the scaling (33) reveals that coalescence of drops with $\lambda = O(1)$ may occur. Coalescence of larger, micron-sized drops requires smaller shear rates. By estimating the diffusion constant for surfactant molecules from Einstein's law as $D = kT/(\mu b)$, where b is the size of surfactant molecule, and by taking $b \approx 10^{-9}$m and $kT \approx 10^{-20}$ J, we obtain $D \approx 10^{-14}$m^2/s and $Pe \approx 1$, which indicates that diffusion may be neglected only for very large surfactant molecules or drops, or at very large shear rates.

III. NUMERICAL METHODS

A. Finite-element formulation

We use the finite element method to solve the flow equations (23) for velocity and pressure [15] and the convection-diffusion equation (29) for bulk concentration. The volume domain is discretized using an unstructured mesh of tetrahedra; the drop-matrix interface is discretized using triangles, that coincide to faces of the tetrahedra. We use a Pressure-Stabilized Petrov-Galerkin formulation [16], and recast the equations in weak form after integration over the bulk domain:

$$\int_\Omega \phi^i (\nabla \cdot \mathbf{T} + \mathbf{f}) \, d\Omega = 0 \tag{34}$$

$$\int_\Omega \phi^i \nabla \cdot \mathbf{u} \; d\Omega + \delta \sum_j \zeta_j^2 \int_{\Delta_j} \nabla \phi^i \cdot \nabla p \; d\Omega = 0 \tag{35}$$

$$\int_{\Omega_m} \phi^i \left(\frac{\partial C}{\partial t} + (\mathbf{u} - \mathbf{u}_e) \cdot \nabla C - Pe^{-1} \nabla^2 C \right) \; d\Omega = 0 \tag{36}$$

where Ω_m is the matrix domain, Ω is the sum of drop and matrix domains, ϕ^i is a piecewise linear basis function for node i, ζ_j is a measure of the size of tetrahedron Δ_j ($\zeta_j = (|\triangle_j|/6)^{1/3}$, where $|\triangle_j|$ is the volume of Δ_j), δ is a pressure-stabilization factor [16] ($\delta = 0.25$ in our implementation), and $\mathbf{u}_e$ is an elemental velocity [17, 18] used to move the tetrahedral mesh while preserving its quality, as described below. The unknowns $\mathbf{u}$, p, C are approximated by

$$\mathbf{u}(\mathbf{x}) = \sum_i \mathbf{u}_i \phi^i(\mathbf{x}), \qquad p(\mathbf{x}) = \sum_i p_i \phi^i(\mathbf{x}), \qquad C(\mathbf{x}) = \sum_i C_i \phi^i(\mathbf{x}), \tag{37}$$

since pressure stabilization allow us to use one linear basis function for all the variables [16].

After integration by parts to lower the order of the derivatives, equations (34) and (36) are rewritten as:

$$\int_\Omega \nabla \phi^i \cdot \mathbf{T} \; d\Omega - \int_\Sigma \phi^i \frac{1}{Ca} (\sigma \kappa \mathbf{n} - \nabla_s \sigma) \; dS - \int_\Omega \phi^i \mathbf{f} \; d\Omega = \mathbf{0} \tag{38}$$

$$\int_{\Omega_m} \phi^i \left(\frac{\partial C}{\partial t} + (\mathbf{u} - \mathbf{u}_e) \cdot \nabla C \right) \; d\Omega + \int_{\Omega_m} \nabla \phi^i \cdot Pe^{-1} \nabla C \; d\Omega + \int_\Sigma \phi^i q_f \; dS = 0 \tag{39}$$

In the above equations, the boundary conditions (26) and (30) have been used to evaluate the surface integrals (and no chemical reaction is considered at the interface).

The volume integrations in (38) and (39) are calculated using 4-point Gaussian quadrature, whereas the surface integrations are calculated using the following method:

$$\int_S \phi(\mathbf{x}) dS = \sum_i \phi(\mathbf{x}_i) \triangle S_i \tag{40}$$

with

$$\triangle S_i = \frac{1}{3} \sum_j \triangle S_{ij} \tag{41}$$

where the index i loops over all surface nodes and the index j loops over all surface elements (triangles) neighbors to node i. $\triangle S_{ij}$ is the area of the surface element j neighbor to node i. The curvature, normal vector and surface gradient are calculated using paraboloid fits [19].

The above residual equations (35), (38) and (39) are put into matrix form using the representation (37) and the quadrature rules listed above. The resulting system of equations is solved using GMRES iterative method [20] with diagonal preconditioning.

B. Time evolution

At each time step, the interface mesh is moved according to the kinematic boundary condition:

$$\frac{\mathrm{d}\mathbf{x}_s}{\mathrm{d}t} = \mathbf{u}(\mathbf{x}_s), \tag{42}$$

where the Lagrangian variable $\mathbf{x}_s$ is node position on the interface. Once the interface movement is calculated, the movement of bulk mesh is computed using a pseudo-solid method previously developed [17, 18] and hence $\mathbf{u}_e$ is determined. Note that the elemental (mesh) velocity $\mathbf{u}_e$ and fluid velocity $\mathbf{u}$ are different in general, except on the drop-matrix interface.

To evolve the drop interfaces and the surface and bulk concentrations of surfactant from time t_n to time t_{n+1}, the following second-order Runge-Kutta (predictor-corrector) scheme is used:

1. Solve the flow equations (35) and (38) for $\mathbf{u}^n$, p^n.

2. Update the interface position:

$$\mathbf{x}_s^{n+1/2} = \mathbf{x}_s^n + \mathbf{u}^n \triangle t/2.$$

3. Update the surface concentration:

$$\Gamma^{n+1/2} = \left(\Gamma^n A^n + \frac{1}{cK} q_f^n \frac{\triangle t}{2} A^n \right) / A^{n+1/2},$$

   where $A \equiv \triangle S_i$ at node i, and the above equation is equivalent to (28) with no diffusion.

4. Solve for the bulk concentration by the FEM:

$$\int_\Omega \phi^i \left(\frac{C^{n+1/2} - C^n}{\triangle t/2} + (\mathbf{u}^n - \mathbf{u}_e^n) \cdot \nabla C^{n+1/2} \right) \, d\Omega$$
$$+ \int_\Omega \nabla \phi^i \cdot Pe^{-1} \nabla C^{n+1/2} \, d\Omega + \int_\Sigma \phi^i q_f^{n+1/2} \, dS = 0$$

5. Solve the flow problem for $\mathbf{u}^{n+1/2}$, $p^{n+1/2}$.

6. Update the interface position using the mid-point value:

$$\mathbf{x}_s^{n+1} = \mathbf{x}_s^n + \mathbf{u}^{n+1/2} \triangle t.$$

7. Update the surface concentration:

$$\Gamma^{n+1} = \left(\Gamma^n A^n + \frac{1}{cK} q_f^{n+1/2} \triangle t A^{n+1/2} \right) / A^{n+1}.$$

8. Solve for the bulk concentration by the FEM:

$$\int_\Omega \phi^i \left(\frac{C^{n+1} - C^n}{\triangle t} + (\mathbf{u}^{n+1/2} - \mathbf{u}_e^{n+1/2}) \cdot \nabla C^{n+1} \right) \, d\Omega + \int_\Omega \nabla \phi^i \cdot Pe^{-1} \nabla C^{n+1} \, d\Omega + \int_\Sigma \phi^i q_f^{n+1} \, dS = 0$$

Step 1 to 4 are prediction steps, and step 5 to 8 are correction steps. Note that although the overall time integration scheme is explicit, the integration for bulk concentration is semi-implicit to increase stability.

C. Mesh generation and adaptive remeshing

We use a commercial software (HyperMesh [21, 22]) to generate the tetrahedral finite element mesh at each time-step of the simulation. This software uses an advancing-front algorithm coupled to a mesh-node volume density function and to Delaunay-based edge swapping techniques to produce a good quality mesh starting from the discretization of the boundaries. In our problem, the boundaries are the drop/matrix interfaces and an outer cubic box (of side length $20a$), which remains fixed during a simulation and delimits the matrix fluid. The boundaries are discretized using a triangulated mesh.

The triangulated interfacial mesh (of input to HyperMesh) is reconstructed at each time-step of simulation using the adaptive remeshing method developed by Cristini *et al.* [23]. This method uses local remeshing operations (e.g., edge swapping, node insertion and removal, and dynamic spring-like node displacement) that reconstruct the mesh according to a desired mesh-node surface density function (nodes per unit surface) that resolves the local curvature and the drop-drop separation. The density function used here is, from Ref. [23],

$$\left(\kappa_1^2 + \kappa_2^2\right)^{\frac{1}{2}} \max\left(\left(\kappa_1^2 + \kappa_2^2\right)^{\frac{1}{2}}, h^{-1} \right), \tag{43}$$

that resolves the smallest length scale set locally either by curvature or by the distance between the drop surfaces in near contact (κ_1 and κ_2 are maximum and minimum dimensionless curvatures, and h is the dimensionless local separation between the drop surfaces).

Adaptivity of the computational mesh allows us to resolve the physical scales and thus to accurately describe the drop evolution and the onset of coalescence.

Between time-steps both the surface and the bulk concentrations Γ and C are mapped from the old mesh to the new mesh and calculated by interpolation. We use an efficient 1-D searching algorithm to locate the element in the old mesh where a given node in the new mesh lies [24].

D. Computational accuracy and efficiency

We parallelized the finite-element algorithm described above. Briefly, a domain decomposition of the finite-element mesh is performed using a public partitioning software (METIS [25]). Partitioning "by dual" is used to obtain an element partitioning and a node partitioning. In the simulations, the element-based (tetrahedra) data structure is used in the calculation of residuals and Jacobians, whereas the node-based data structure is used in solving the linear system of equations. Communications among different partitions are performed using a Message Passing Interface as described in Ref. [26]. This parallelization allows us to obtain almost linear speed up. The speed up in CPU time from 1 processor to 2 processors was 1.93, and from 2 processors to 4 processors was 1.82. Note that because we remesh at every step, we need to redo mesh partitioning and other book keeping at every step, which makes the scaling a little worse. In problems with fixed mesh topology, we have achieved speed up of 1.91 from 32 to 64 and from 64 to 128 processors [26].

IV. RESULTS AND DISCUSSION

A. Effect of surfactant on pair interactions

In Figure 1 (a) and (b), two sequences of pair interactions are illustrated corresponding to capillary number $Ca = 0.11$ and 0.12 respectively. The nondimensional minimal drop-drop separation h/a is also plotted in Figure 1 (c) as a function of the horizontal offset $\triangle x/a$. As the drops are deformed and pushed towards each other by the shear flow, surfactant redistribution occurs: the surfactant molecules are convected towards the drop tips. As the drops become closer to each other, the high pressure that develops in the gap pushes surfactant away from the near-contact region, thus generating Marangoni stresses that oppose

further approach. For $Ca = 0.11$, the interaction time is long enough that the gap narrows to a value $h/a \approx 0.02$ where attractive van der Waals forces dominate repulsive hydrodynamic and Marangoni forces, and coalescence occurs. For $Ca = 0.12$, the hydrodynamic and Marangoni forces prevent the drops from getting close enough to trigger the van der Waals attraction. Note the higher value of surfactant redistribution ($\Gamma_{max} \approx 1.86$ in Figure 1 (b) vs. $\Gamma_{max} \approx 1.57$ in Figure 1 (a); $\Gamma = 1$ initially). Consequently, for $Ca = 0.12$ the drop separation reaches a minimum and then increases again. Coalescence does not occur. The results presented in Figure 1 allow us to determine the range for critical capillary number: $0.11 < Ca_c < 0.12$.

In the absence of surfactant, our simulations (not shown) reveal that higher capillary numbers are required to prevent coalescence. This can be understood through the following scalings [2, 3], although limited to very small capillary numbers for which the drops remain nearly spherical during their interaction. At small drop-drop separations $h \ll a$, a high repulsive lubrication pressure p arises in the gap, and balances the force $F \sim \mu\dot{\gamma}a^2$ of the flow. It can be shown by a lubrication approximation for spherical drops that the surface area over which the lubrication pressure develops scales as ah. Thus the scaling $p \sim F/(ah)$ holds. If surfactants are present, additional pressure comes from the flow induced by Marangoni stresses $\Delta\sigma/(ah)^{\frac{1}{2}}$, where $\Delta\sigma$ is the absolute variation in surface tension in the near-contact region due to surfactant redistribution. It can be shown by a force balance in the gap that the pressure due to Marangoni stresses scales as $\Delta\sigma/h$ and thus the total pressure in the gap is $p \sim F/(ah) + \Delta\sigma/h$. As this lubrication pressure equates the capillary pressure σ_e/a, the near-contact region begins to deform. Typically, a dimple forms strongly preventing further approach of the drops and coalescence. The gap at which this happens is obtained by equating $p \sim \sigma_e/a$, thus giving

$$h/a \sim \frac{F}{\sigma_e a} + \frac{\Delta\sigma}{\sigma_e} = Ca + \frac{\Delta\sigma}{\sigma_e}. \tag{44}$$

Thus in the presence of surfactants lower capillary numbers are required to prevent coalescence thanks to the additional repulsive effect of Marangoni stresses.

In Figure 2, the effect of surfactant solubility (in the matrix fluid) is shown for $Ca = 0.12$ (cf. Figure 1 (b)). Bulk diffusion decreases Marangoni stresses by redistributing the surfactant through desorption from the drop ends and adsorption in the middle regions of the drops ($\Gamma_{max} \approx 1.33$ in Figure 2 vs. $\Gamma_{max} \approx 1.86$ in Figure 1 (b)). Thus, repulsive

Marangoni forces are smaller than in the insoluble case, and coalescence is favored with respect to the insoluble-surfactant case.

The computational meshes corresponding to Figure 2 are shown in Figure 3. Figure 3(a) and (b) show planar slices of the volume mesh of tetrahedra discretizing the matrix fluid, and the triangulated 3D mesh discretizing the drop-matrix interfaces, at the beginning ($\dot{\gamma}t = 0$) and at the onset of coalescence ($\dot{\gamma}t = 6.4$). Figure 3(c) shows a blow up of the near-contact region: a planar slice of the tetrahedra discretizing both the matrix and drop fluids at the onset of coalescence (the matrix is darkly shaded and the drops are lightly shaded). The elements may appear skewed as an artifact of projecting the 3D elements on a 2D planar slice. As with most of the simulations (except those for refinement studies), the initial number of nodes (at time $t = 0$) on each drop surface is $N_0 = 100$. The total initial numbers of nodes and elements in the whole computational domain are 2413 and 13591 respectively. As a consequence of mesh adaptivity, the number of nodes increases as drops deform and as they get closer to each other according to the density function (43). At the onset of coalescence, the number of nodes on each drop surface has changed to $N = 272$. and the total numbers of nodes and elements have increased to 2668 and 15060 respectively. Refinement has occurred only in the near-contact regions of the drop surfaces and in regions of high curvature. Thus, the total computational expense remains affordable.

B. Critical capillary numbers for coalescence

In Figure 4, critical conditions for coalescence are reported as a function of the Hamaker number for the case $c = 0$, i.e., no surfactant is present. Each pair of points corresponds to two simulations: coalescence occurs for the lower value of capillary number and does not occur for the higher. Thus, the critical capillary number lies in between. As the Hamaker number increases, van der Waals forces are stronger and thus coalescence becomes possible at higher capillary numbers in spite of a larger drop deformation. The straight lines are fits through the data with slope of 2/9 corresponding to the scaling in equation (33), thus in agreement with the lubrication theory [1]. The deviation of the numerical results from the straight line at the highest capillary numbers can be explained considering that those points correspond to conditions close to break-up (which occurs at $Ca \approx 0.4$ for the lower accuracy used) where the drop deformation is large and the lubrication approximation [1]

does not apply. In Figure 4, triangles, squares and circles denote simulations corresponding to $N_0 = 100$, 200 and 400 respectively, where N_0 is the initial number of nodes on each drop surface. The constancy of the slope between simulations with different mesh resolutions shows that the prediction of the slope is quite accurate. The refinement study in Figure 5 shows linear convergence of Ca_c with $1/N_0$. However, the value of critical capillary number has large error (nearly 50% at the lowest resolution). Performing more accurate simulations was limited by computational expense.

The effect of surfactant concentration on Ca_c is illustrated in Figure 6. The two curves labelled "insoluble" represent the critical capillary number as a function of surfactant coverage for two different Hamaker numbers and for a surfactant insoluble in the bulk. The critical capillary numbers are estimated as the mean points of data pairs analogous to those in Figure 4. The results reveal a nontrivial dependence on the surfactant coverage. At small coverages, Marangoni stresses prevent drop approach resulting in the decrease of the critical capillary numbers for coalescence with respect to the clean-drops ($c = 0$) case. However, as the surfactant coverage increases, the critical capillary number reaches a minimum (at $c \approx 0.75$) and then increases again. This nontrivial behavior was first reported by Leal and coworkers [7] from experiments under different flow conditions. In one case in our simulations ($c = 0.98$ and $Ha = 10^{-4}$) Ca_c is even larger than the value for clean surfaces.

The reason for this non-monotonic behavior rests on the nontrivial dependence of Marangoni stresses and drop deformation on the surfactant coverage. In Figure 7 (lines), Marangoni stresses and drop deformations are reported for $Ha = 10^{-4}$ at various surfactant coverages and capillary number $Ca = 0.20$, which is near the critical at $c = 0$. Marangoni stresses are estimated by the maximum difference in surface tension on the drop surfaces during drop interactions. Likewise the area ratio represents the maximum surface area during drop interaction divided by the undeformed area. Note that the total area change, even for near-coalescence conditions, is not large, less than 5%. But deformation in the near-contact region is sufficient to prevent coalescence. As shown in Figure 7, both Marangoni stresses and drop deformation increase with c and reach a maximum at $c \approx 0.75$. Correspondingly, coalescence is hindered and the critical capillary number reaches a minimum (cf. Figure 6). However, as $c \to 1$ the surfactant becomes nearly incompressible and does not redistribute. Thus both Marangoni stresses and drop deformation decrease. As a consequence, coalescence becomes possible at higher capillary numbers and Ca_c increases. Figure 7 (bottom)

reveals that at $c = 0.98$ the drops are less deformed than clean drops ($c = 0$), and thus the critical capillary number at $c = 0.98$ is even higher than that at $c = 0$ (cf. Figure 6 (dashed line)).

In Figure 6 the effect of solubility in the matrix fluid is also shown ("soluble" curve). At $c = 0$, no surfactants are present, and the curves "soluble" and "insoluble" coincide (for the same Hamaker number). For $c > 0$, the critical capillary number for coalescence is at first significantly increased by solubility with respect to the insoluble case. This is mainly a consequence of diffusion in the matrix fluid that counteracts surface redistribution and thus weakens Marangoni stresses. However, as c increases, the difference in Ca_c between soluble and insoluble cases decreases, and the two curve eventually cross each other. For $c > 0.9$, Ca_c is actually reduced by solubility. This nontrivial effect is explained in Figure 7, in which Marangoni stresses and drop deformations are compared in the soluble (circles) and insoluble (triangles) cases for two values of c. At $c = 0.5$, Marangoni stresses are significantly decreased by solubility, and thus Ca_c is increased. In contrast at $c = 0.95$ the large bulk equilibrium concentration results in large adsorption fluxes that maintain a higher amount of surfactant on the surfaces than in the insoluble case. Thus drop deformation is significantly increased (Figure 7 (bottom)) inhibiting coalescence and reducing the critical capillary number for coalescence with respect to the insoluble case.

V. CONCLUSIONS

We have developed a robust, efficient and versatile 3D adaptive numerical method for simulations of multiphase flows of interest to rheology. We have applied our method to investigate the effects of soluble and insoluble surfactants on drop-drop collisions and coalescence in shear flow.

We have demonstrated nontrivial dependence of conditions for coalescence (critical capillary number) on the surfactant coverage on the interfaces. Marangoni stresses increase drop-drop repulsion and hinder coalescence at low surfactant concentrations. However, at high concentrations surfactant becomes nearly incompressible weakening Marangoni stresses and drop deformation and thus allowing coalescence at higher capillary numbers. Steric effects associated to the finite size of the surfactant molecules, and neglected here, may make block copolymers effective at preventing coalescence [8] even at high Ca. Steric effects will

be included as part of our future work by appropriately modifying the force law $\mathbf{f}$ in equation (1).

We have also found a nontrivial effect of the surfactant concentration in the matrix fluid. Solubility in the bulk hinders coalescence by redistributing surfactant to decrease gradients of concentration thus weakening Marangoni stresses and increasing the critical capillary number with respect to the insoluble-surfactant case. However, at high bulk concentration, high adsorption fluxes maintain a higher coverage of surfactant on the drop surfaces, thus lowering surface tension, increasing drop deformation and preventing drop-drop approach. Consequently, at high surfactant concentrations the critical capillary number for coalescence is lower than in the insoluble case.

As part of future work we will investigate the effects of soluble and insoluble surfactants on the breakup mechanism and on the resulting fragment size distributions.

Acknowledgments

The authors acknowledge partial support by Army Research Office, Department of Energy (Division of Basic Energy Sciences) and National Science Foundation (Division of Mathematics) grants. The authors also acknowledge the Institute for Mathematics and its Applications for its hospitality and the Minnesota Supercomputing Institute (MSI) for computational time and support. VC also acknowledges the MSI for a research scholarship.

---

[1] A. K. Chesters. The modelling of coalescence processes in fluid liquid dispersions–a review of current understanding. *Trans. Inst. Chem. Eng.*, 69:259, 1991.

[2] V. Cristini, J. Bławzdziewicz, and M. Loewenberg. Near-contact motion of surfactant-covered spherical drops. *J. Fluid Mech.*, 366:259, 1998.

[3] J. Bławzdziewicz, V. Cristini, and M. Loewenberg. Near-contact motion of surfactant-covered spherical drops: Ionic surfactant. *J. Coll. Int. Sci.*, 211:355, 1999.

[4] J. Bławzdziewicz, V. Cristini, and M. Loewenberg. Stokes flow in the presence of a planar interface covered with incompressible surfactant. *Phys. Fluids*, 11:251, 1999.

[5] A. K. Chesters and I.B. Bazhlekov. Effect of insoluble surfactants on drainage and rupture of a film between drops interacting under a constant force. *J. Coll. Int. Sci.*, 230:229, 2000.

[6] S. T. Milner and H. Xi. How copolymers promote mixing of immiscible homopolymers. *J. Rheol.*, 40:663, 1996.

[7] Y.T. Hu, D.J. Pine, and L. G. Leal. Drop deformation, breakup, and coalescence with compatibilizer. *Phys. Fluids*, 12:484, 2000.

[8] S. Lyu, T. D. Jones, F. S. Bates, and C. W. Macosko. Role of block copolymers on suppression of droplet coalescence. *Macromolecules*, 35:7845–7855, 2002.

[9] W. B. Russel, D. A. Saville, and W. R. Schowalter. *Colloidal Dispersions*. Cambridge University Press, New York, 1989.

[10] Y. Pawar and K. J. Stebe. Marangoni effects on drop deformation in an extensional flow: The role of surfactant physical chemistry. I. insoluble surfactants. *Phys. Fluids*, 8(7), 1996.

[11] H. A. Stone. A simple derivation of the time dependent convection diffusion equation for surfactant transport along a deforming interface. *Phys. Fluids A*, 2:111–112, 1990.

[12] H. Wong, D. Rumschitzki, and C. Maldarelli. On the surfactant mass balance at a deforming fluid interface. *Phys. Fluids A*, 8:3203–3204, 1990.

[13] B. Cuenot, J. Magnaudet, and B. Spennato. The effect of slightly soluble surfactants on the flow around a spherical bubble. *J. Fluid Mech.*, 339:25–53, 1997.

[14] C. D. Eggleton, T. M Tsai, and K. J. Stebe. Tip streaming from a drop in the presence of surfactants. *Phys. Rev. Let.*, 87(4), 2001.

[15] R. Hooper, V. Cristini, S. Shakya, J. Lowengrub, C.W. Macosko, and J. J. Derby. Modeling multiphase flows using a novel 3d adaptive remeshing algorithm. In *Computational methods in multiphase flow*, Wessex Institute of Technology Press, UK, 2001.

[16] T. J. R. Hughes, L. P. Franca, and M. Balestra. A new finite element formulation for computational fluid dynamics: V. Circumventing the Babuška-Brezzi condition: A stable Petrov-Galerkin formulation of Stokes problem accomodating equal-order interpolations. *Computer Meth. Appl. Mech. Eng.*, 59:85–99, 1986.

[17] Hua Zhou and Jeffrey J. Derby. An assessment of a parallel, finite element method for three-dimensional, moving-boundary flows driven by capillarity for simulation of viscous sintering. *Int. J. Numer. Meth. Fluids*, 36:841–865, 2001.

[18] P. A. Sackinger, P. R. Schunk, and R. R. Rao. A Newton-Raphson pseudo-solid domain

mapping technique for free and moving boundary problems: A finite element implementation. *J. Comp. Phys.*, 125:83–103, 1996.

[19] A. Z. Zinchenko, M. A. Rother, and R. H. Davis. A novel boundary-integral algorithm for viscous interaction of deformable drops. *Phys. Fluids*, 9(6):1493–1511, 1997.

[20] Y. Saad and M. Schultz. GMRES: A generalized minimum residual algorithm for solving nonsymmetric linear systems. *SIAM J. Sci. Stat. Comput.*, 7:856–69, 1986.

[21] D. L. Marcum and N. P. Weatherill. Unstructured grid generation using iterative point insertion and local reconnection. *AIAA J.*, 33:1619, 1995.

[22] D. L. Marcum. Adaptive unstructured grid generation for viscous flow applications. *AIAA J.*, 34:2440, 1996.

[23] V. Cristini, J. Blawzdziewicz, and M. Loewenberg. An adaptive mesh algorithm for evolving surfaces: simulations of drop breakup and coalescencez. *J. Comp. Phys.*, 168:445–463, 2001.

[24] A. A. Johnson and T. E. Tezduyar. 3D simulation of fluid-particle interactions with the number of particles reaching 100. *Computer Meth. Appl. Mech. Eng.*, 145(3–4):301–321, 1997.

[25] George Karypis and Vipin Kumar. Multilevel k-way partitioning scheme for irregular graphs. *J. Parallel Distributed Comput.*, 48:96–129, 1998.

[26] H. Zhou and J. J. Derby. Parallel implementation of finite element method with MPI: Application to three-dimensional free surface stokes flow. In *Proceedings of International Conference on Parallel and Distributed Processing Techniques and Applications*, Las Vegas, NV, 2000.

(a)

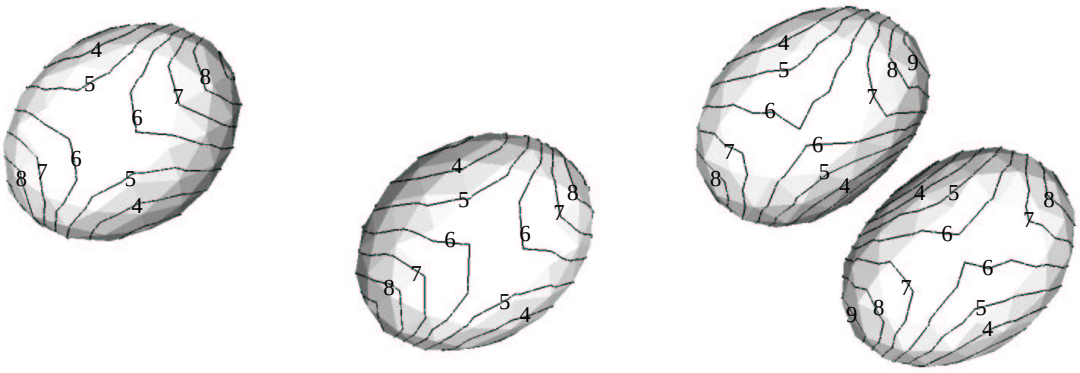

γ=3 γ=5

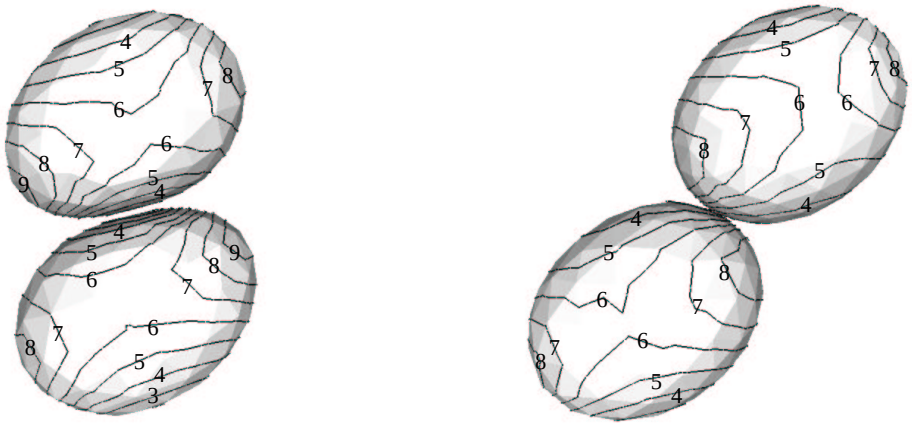

γ=6 γ=6.9

Contour level	1	2	3	4	5	6	7	8	9	10
Γ	0.37	0.50	0.64	0.77	0.90	1.04	1.17	1.30	1.44	1.57

(b)

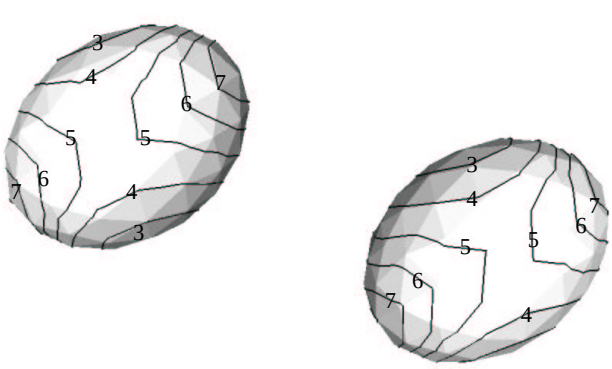

γ=3

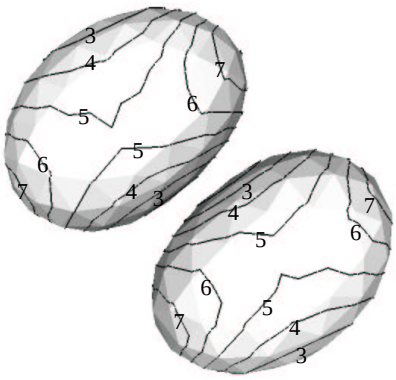

γ=5

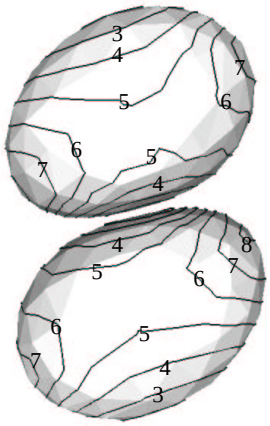

γ=6

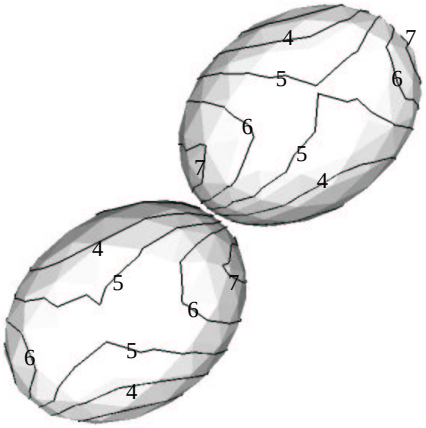

γ=7

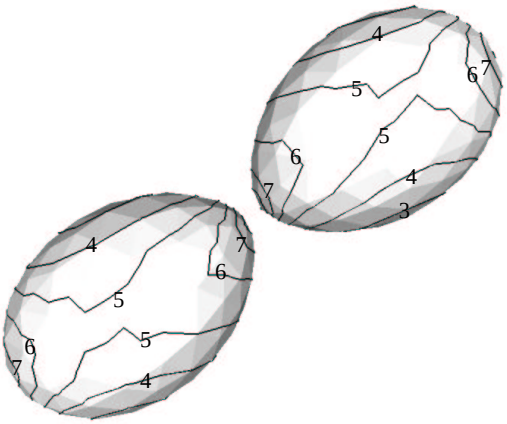

γ=7.5

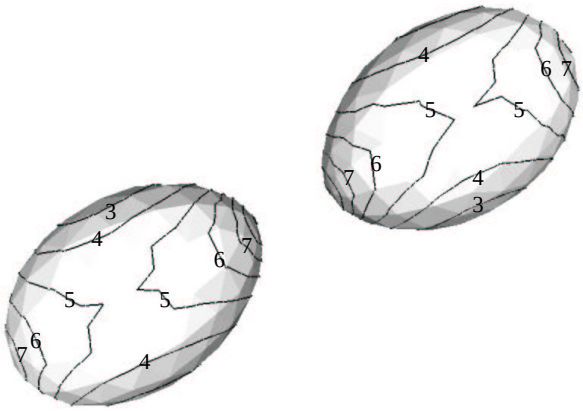

γ=8

Contour level	1	2	3	4	5	6	7	8	9	10
Γ	0.36	0.53	0.69	0.86	1.03	1.19	1.36	1.52	1.69	1.86

(c)

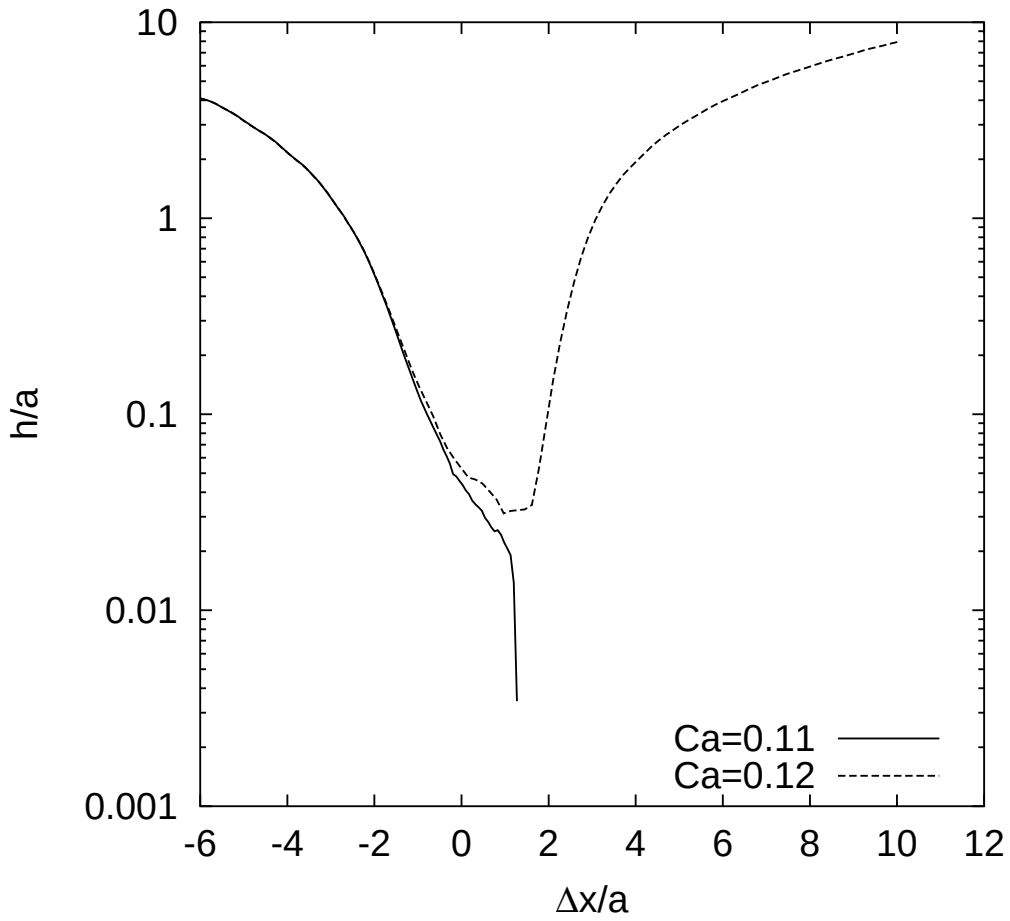

FIG. 1: Pair interactions with insoluble surfactant ($E_0 = 0.2$, $c = 0.5$, $Ha = 10^{-4}$, initial number of computational nodes on each drop $N_0 = 100$, $\lambda = 1$ and initial offsets $\triangle x/a = -6$ and $\triangle y/a = 1$). (a) Sequence of interaction for $Ca = 0.11$ (below critical). Values of strain $\gamma = \dot{\gamma}t$ labelled, illustrating the onset of coalescence at $\gamma = 6.9$. Surfactant concentration Γ is shown by contour levels on the drop surfaces, going from minimum (level 1) to maximum (10) over the entire simulation. (b) Same as in (a), but for $Ca = 0.12$ (above critical): coalescence does not occur. (c) Dimensionless gap h/a (minimal separation between the two drops) as a function of dimensionless horizontal offset $\triangle x/a$. For $Ca = 0.12$, hydrodynamic and Marangoni forces dominate over van der Waals forces and coalescence does not occur; for $Ca = 0.11$, the opposite happens. This implies that the criticality $0.11 < Ca_c < 0.12$. Note for $Ca = 0.11$ the sharp change in the gap thinning rate as van der Waals forces become dominant.

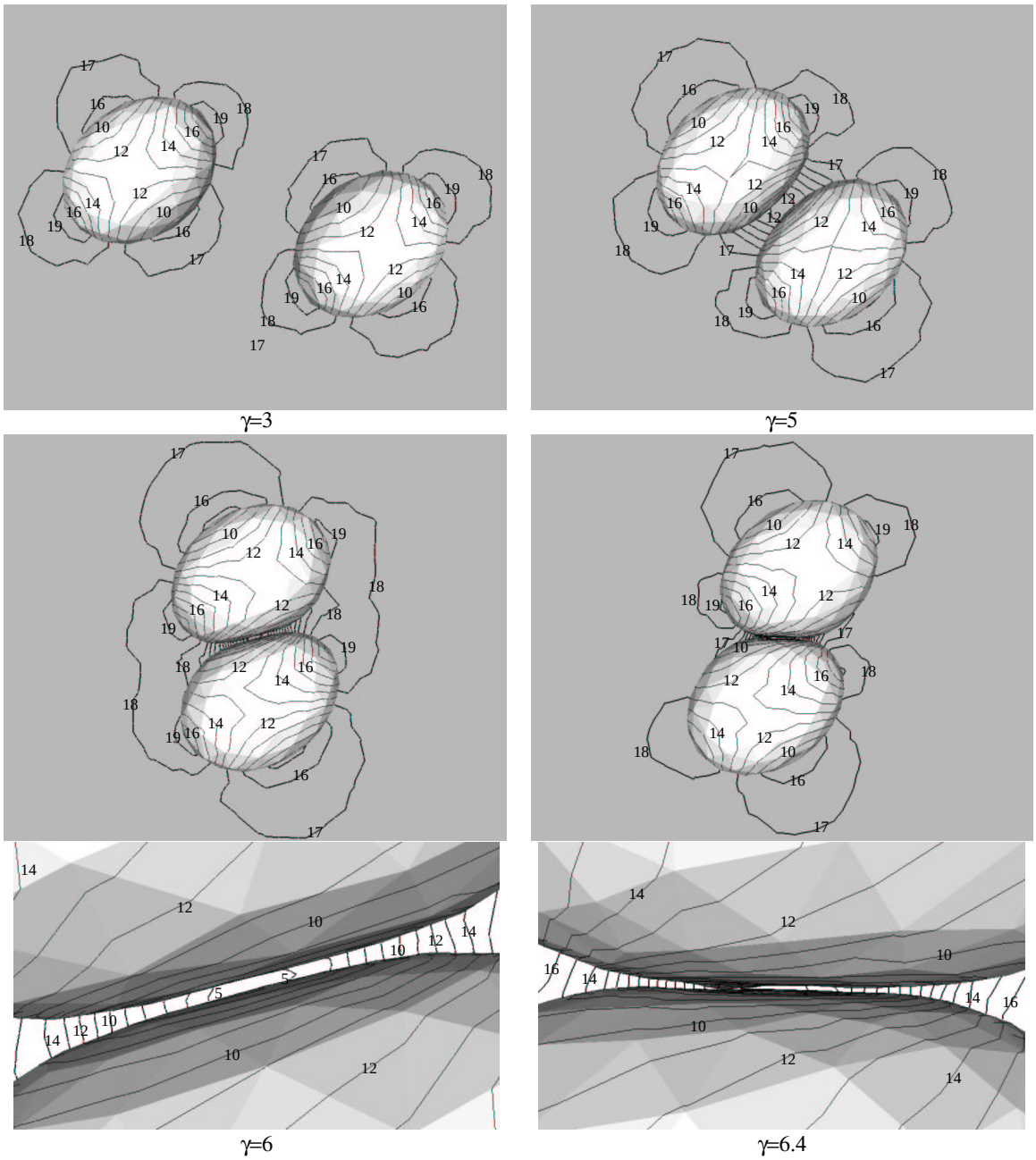

Contour level	1	2	4	6	8	10	12	14	16	18	20
Γ	0.49	0.53	0.62	0.71	0.80	0.89	0.97	1.06	1.15	1.24	1.33
C	0.60	0.62	0.67	0.72	0.77	0.82	0.87	0.92	0.96	1.01	1.06

FIG. 2: Same as in Figure 1 (b), but with a surfactant soluble in the matrix fluid ($\alpha = 1$, $Pe = 1$, $K = 1$). Strain $\gamma = \dot{\gamma}t$ labelled. The drop surfaces and a planar cut through the matrix volume shown. The contour on the plane is for bulk concentration C and the contour on the drop surface is for surface concentration Γ. Contour levels go from minimum (level 1) to maximum (level 20) over the entire simulation. Odd levels (except level 1) are omitted to save space. Here, bulk diffusion strongly reduces surface concentration gradients and Marangoni stresses, and thus coalescence occurs. The last frame shows the onset of coalescence.

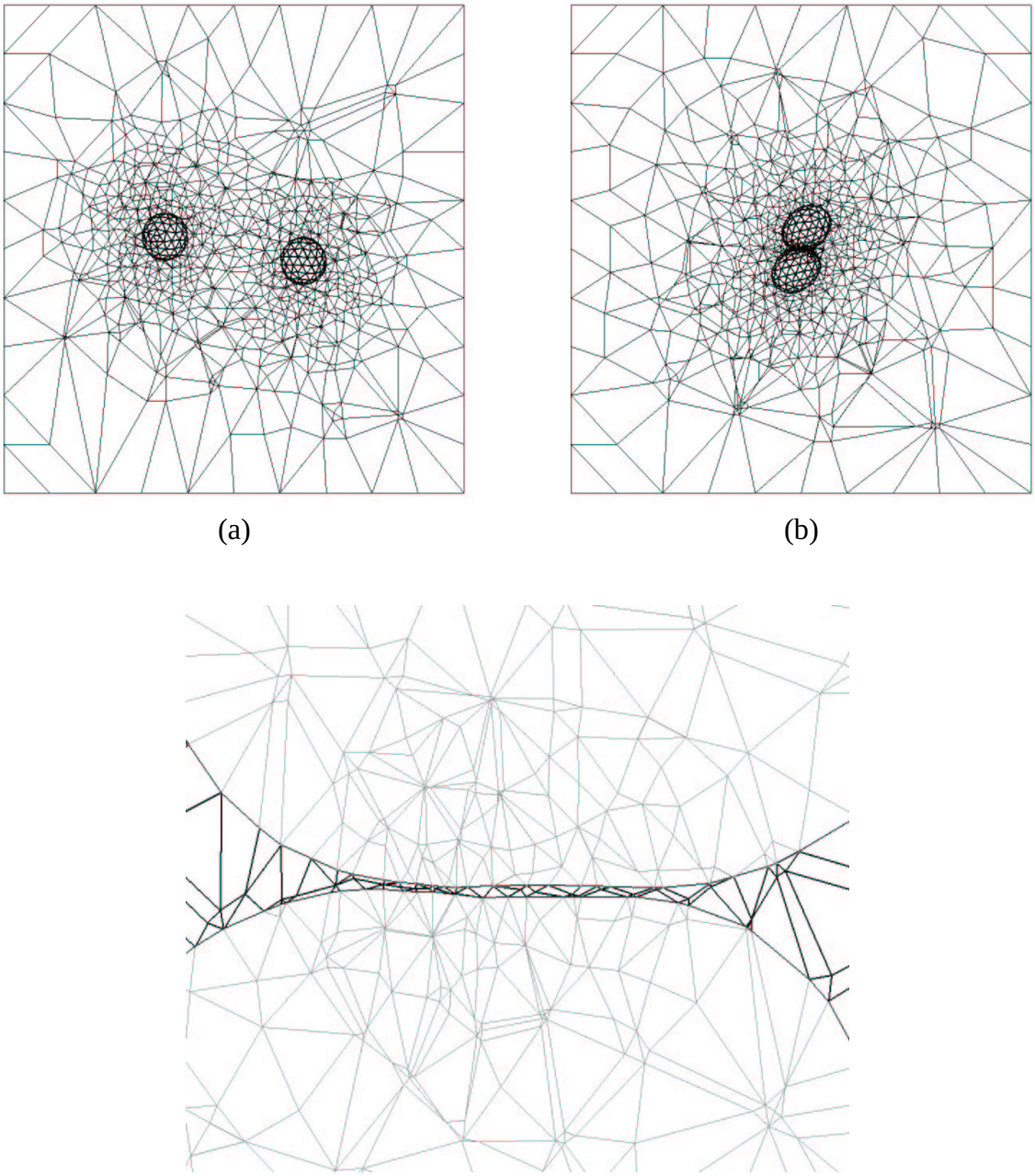

FIG. 3: Computational mesh for the case shown in Fig. 2. (a): $\dot{\gamma}t = 0$. (b) and (c): $\dot{\gamma}t = 6.4$. (a) and (b) show: a 2D planar slice through the 3D mesh of tetrahedra discretizing the matrix; the mesh of triangles discretizing the drop surfaces. (c) shows a blow-up of the 2D slices of the tetrahedral meshes discretizing both matrix (heavily shaded) and drops (lightly shaded) in the near-contact region.

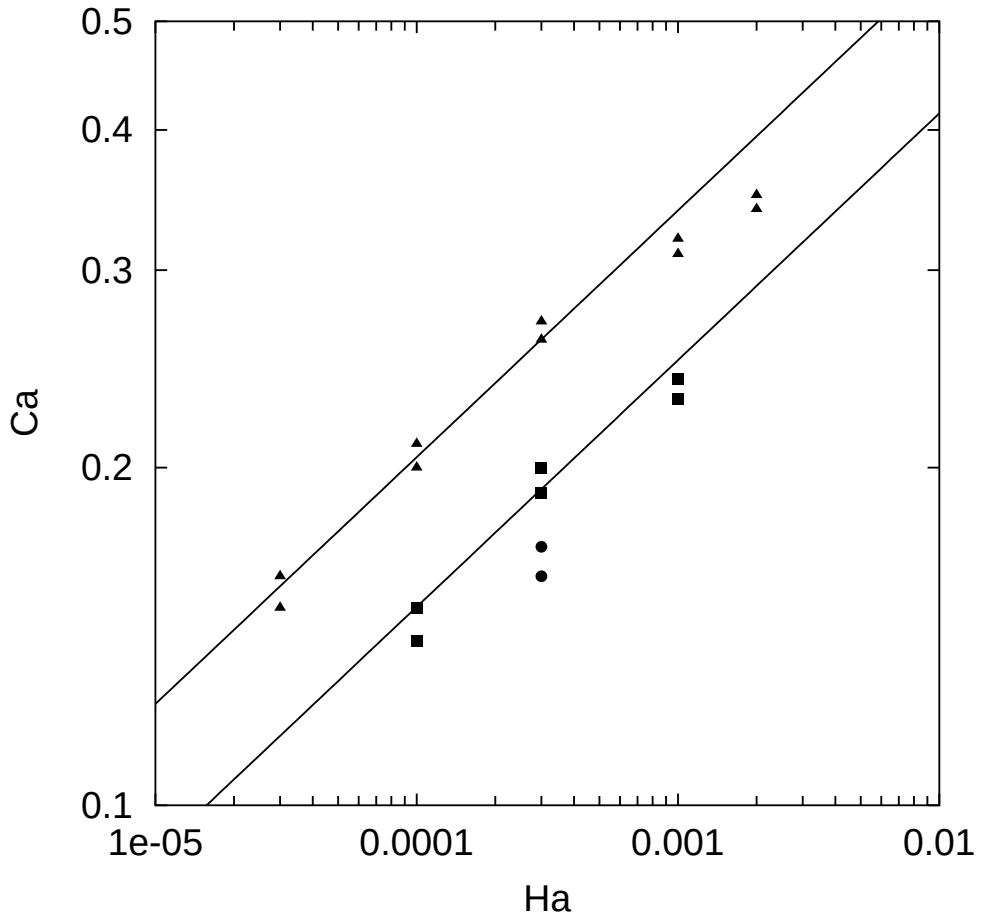

FIG. 4: Critical conditions for coalescence in shear flow as a function of Hamaker number in the absence of surfactant ($c = 0$) and for $\lambda = 1$ and initial offsets $\triangle x/a = -6$ and $\triangle y/a = 1$. Initial number of nodes on each drop surface $N_0 = 100$ (triangles), 200 (squares) and 400 (circles). Each pair of points corresponds to two simulations: coalescence occurs for the lower value of capillary number and does not occur for the higher. The critical capillary number lies in between. The lines are fits with slope 2/9 from the scaling (33).

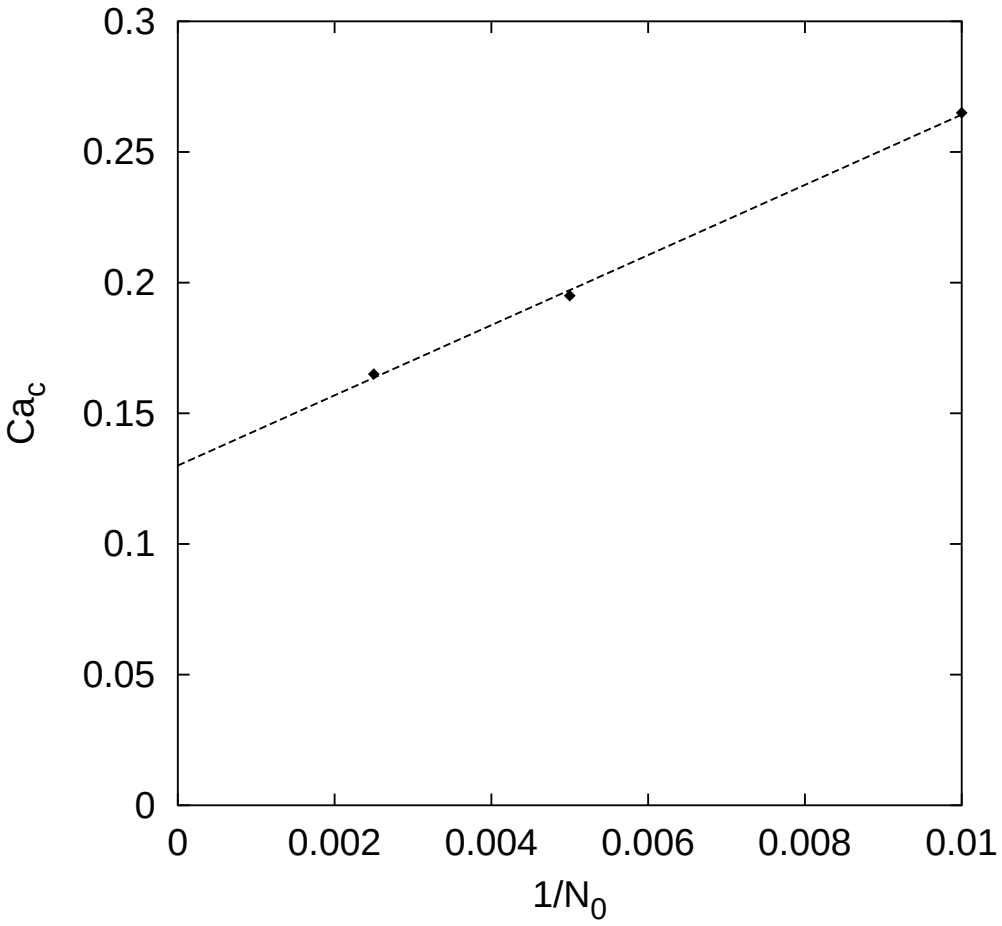

FIG. 5: Critical capillary number Ca_c vs. reciprocal of initial number of nodes $1/N_0$. Symbol: The critical capillary numbers determined by the average of the simulation pairs shown in Figure 4. Line: linear fit demonstrating $O(1/N_0)$ convergence.

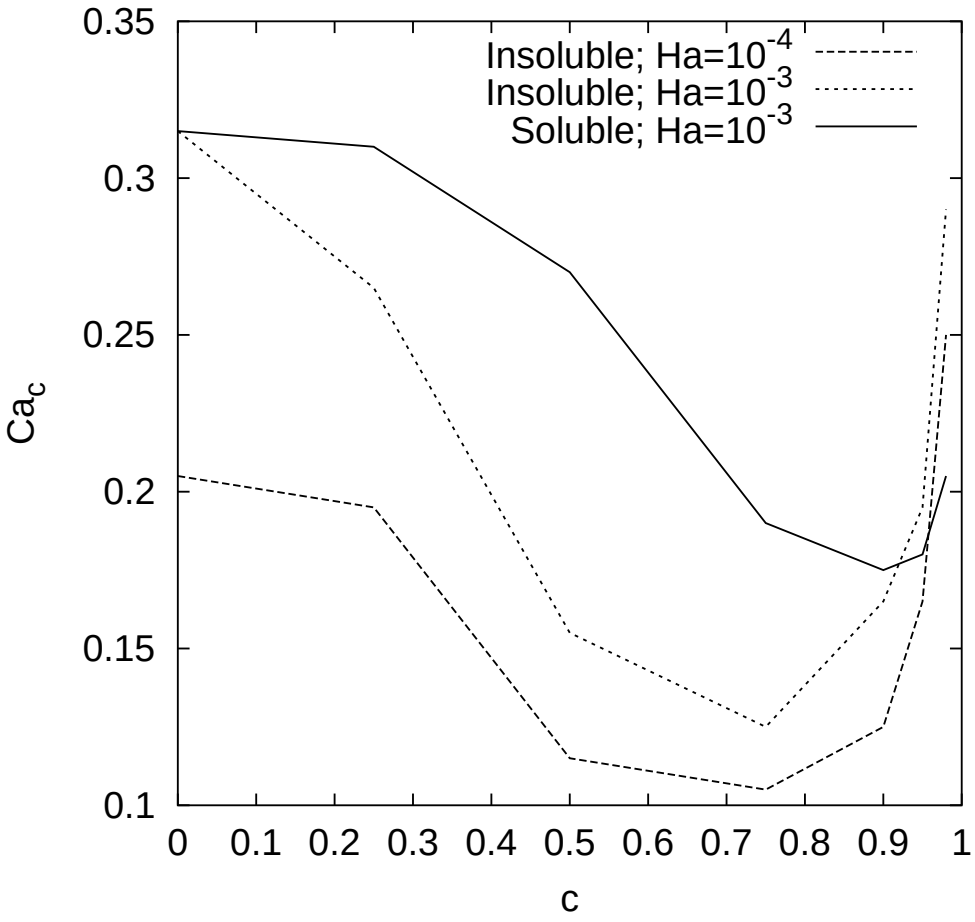

FIG. 6: Critical capillary number Ca_c as a function of initial surfactant coverage c for two different Hamaker numbers and for both soluble (in the matrix fluid only) and insoluble surfactant ($E_0 = 0.2$, $\lambda = 1$, initial offsets $\triangle x/a = -6$ and $\triangle y/a = 1$, initial number of nodes $N_0 = 100$; for the soluble case $\alpha = 1$, $Pe = 1$, and $K = 1$). The estimates for Ca_c are obtained as the mid-points of the results from simulation pairs (cf. Figure 4). These results reveal a nontrivial dependence of critical capillary number on the surfactant coverage.

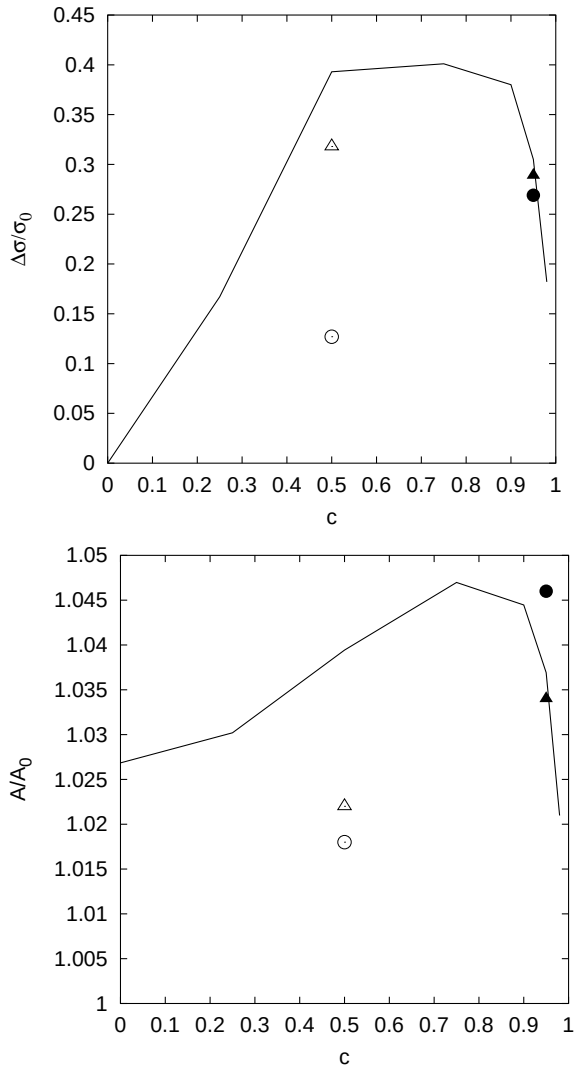

FIG. 7: Lines: Maximum difference in surface tension (top) and maximum surface area A/A_0 (bottom, where A_0 is the initial drop area) during pair interactions with insoluble surfactant ($Ha = 10^{-4}$, $Ca = 0.20$). Symbols: comparison between insoluble (triangles) and soluble (circles) cases (for $Ha = 10^{-3}$ and capillary numbers $Ca = 0.15$ (open) and 0.19 (filled) just below the "insoluble" curve in Figure 6).